CFD analysis of phase-change material-based heat storage with dimple-shaped fins: evaluation of fin configuration and distribution pattern

Nidhal Ben Khedher[1,2], Jasim M. Mahdi [ID][3,*], Hasan S. Majdi[4], Koorosh Khosravi[5], Waleed Khalid Al-Azzawi[6], Fadhil Abbas Al-Qrimli[7], Sami Dhahbi[8] and Pouyan Talebizadehsardari[9]

[1]Department of Mechanical Engineering, College of Engineering, University of Ha'il, P.O. Box 2440, Ha'il City, Saudi Arabia
[2]Laboratory of Thermal and Energetic Systems Studies (LESTE) at the National School of Engineering of Monastir, University of Monastir, 50000, Tunisia
[3]Department of Energy Engineering, University of Baghdad, Baghdad 10071, Iraq
[4]Department of Chemical Engineering and Petroleum Industries, Al-Mustaqbal University College, Babylon 51001, Iraq
[5]Department of Thermo-fluids Engineering, School of Mechanical Engineering, Shiraz University, Shiraz, Iran
[6]Department of Medical Instrumentation Techniques Engineering, Al-Farahidi University, Baghdad 10015, Iraq
[7]College of Engineering, Uruk University, Baghdad 10069, Iraq
[8]Department of Computer Science, College of Science and Art at Mahayil, King Khalid University, Muhayil Aseer, 62529, Saudi Arabia
[9]Centre for Sustainable Energy Use in Food Chains, Institute of Energy Futures, Brunel University London, Kingston Lane, Uxbridge, Middlesex UB8 3PH, UK
*Corresponding author. E-mail: jasim.m@siu.edu

Abstract

Phase-change materials (PCMs) have a remarkable potential for use as efficient energy storage means. However, their poor response rates during energy storage and retrieval modes require the use of heat transfer enhancers to combat these limitations. This research marks the first attempt to explore the potential of dimple-shaped fins for the enhancement of PCM thermal response in a shell-and-tube casing. Fin arrays with different dimensions and diverse distribution patterns were designed and studied to assess the effect of modifying the fin geometric parameters and distribution patterns in various spatial zones of the physical domain. The results indicate that increasing the number of dimple fins in the range of 8–32 results in faster heat storage rates by up to 8.7% faster than they would be without the dimple fins. Further improvements of approximately 1.4, 1.2, 1.1, and 1.0% can be obtained by optimizing the position of the first fin section, the spacing between other fin sections, the fin spacing based on the aromatic algorithm, and the use of the staggered fin distribution. The heat storage rate is improved by almost 12% for the best case compared with that of the no-fin case.

Keywords: heat storage, thermal enhancement, energy efficiency, dimple fins, shell-and-tube

Nomenclature

A_m:	Mushy zone parameter
C_p (J kg^{-1} K^{-1}):	Specific heat capacity
g (m s^{-2}):	Gravity
k (W m^{-1} K^{-1}):	Thermal conductivity
L_f (J kg^{-1}):	Latent heat of melting
M (kg):	Mass
P (Pa):	Pressure
Q (kJ):	Heat storage
t_m (s):	Melting/solidification time
T (K):	Temperature
S:	Source term
$\overrightarrow{V}$ (m s^{-1}) :	Velocity
Greek symbols:	
β (K^{-1}):	Thermal expansion coefficient
λ :	Liquid fraction
μ (kg m^{-1} s^{-1}):	PCM viscosity
ρ (kg m^{-3}):	PCM density
ΔH (J kg^{-1}):	PCM latent heat

1. Introduction

There is no doubt that the continued harsh use of fossil fuels is the major contributor to global carbon emissions, accounting for more than 80% in industrialized nations (Ritchie *et al.*, 2020). All energy transition plans necessarily entail increasing renewable energy utilization and end-use energy efficiency (Zhang *et al.*, 2016; Wang *et al.*, 2018). However, the vulnerability of renewable energy systems and their high installation costs have been and will continue to be a challenge for scientists and researchers in the energy field (Gong *et al.*, 2022; Xu *et al.*, 2022). Thermal energy storage (TES) is viewed as the major enabler for addressing the vulnerability of renewable energy and facilitating more efficient exploitation of it (Wu *et al.*, 2021a, b). It can secure steady power output from vulnerable energy sources, thus conserving scarce fossil-fuel resources and reducing the need for costly fossil-fuel imports (Dincer & Rosen, 2021; Yang *et al.*, 2021). As a result, it is essential to develop robust designs that precisely match the proper TES technology to their unique renewable energy application (Yang *et al.*, 2022b). TES is basically the process of storing
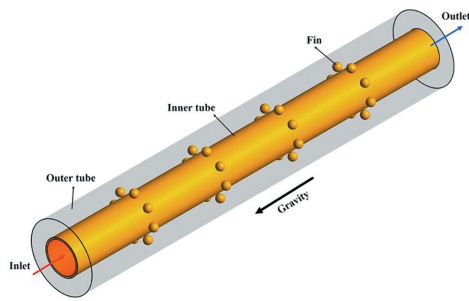
Figure 1: Schematic of the proposed heat exchanger equipped with dimple-shaped fins.

energy thermally for later use. It is categorized into three types based on the materials utilized: These are sensible, latent, and thermochemical TES. The latent TES, which uses phase-change materials (PCMs), is preferred over other types for two reasons. First, PCM-based TES systems are usually smaller than conventional TES systems when the system size is a design concern. For example, the storage density of PCM compared to that of rock TES is about 1–17 (Lane, 1983). Second, the thermophysical nature of phase transitions in PCMs allows for minimal temperature deterioration, allowing for almost constant temperature operation. PCMs are used in a variety of engineering applications, including energy management in buildings (Lamrani *et al.*, 2021), load control in HVAC utilities (Sardari *et al.*, 2019; Dong *et al.*, 2020), and peak shaving in renewable energy systems (Pelay *et al.*, 2017; Rea *et al.*, 2018; Saffari *et al.*, 2018).

Heat transfer rate, phase transition temperature, and latent enthalpy of melting are among the material thermo-physical parameters that mainly contribute to the usefulness of PCMs as heat storage media. While there are significant metallurgical variances between PCMs today, the most prevalent trait is that they all have naturally low thermal conductivities, which has a negative impact on the thermodynamic response to the energy charging and discharging cycles (Cabeza, 2021). To alleviate this challenge, researchers tested and suggested a variety of ways for the thermal response enrichment of TES systems. These ways include capsulation of PCMs, embedding of porous matrices (Mahdi *et al.*, 2021a, b; Talebizadehsardari *et al.*, 2021a), adding extended fin surfaces (Yang *et al.*, 2020; Mahmoud *et al.*, 2021; Sun *et al.*, 2021; Guo *et al.*, 2022; Yang *et al.*, 2022a), incorporating nano-additives (Zhang *et al.*, 2015, 2018), applying multiple-PCMs (Mahdi *et al.*, 2020, 2021c), and heat pipes (Ali, 2019), as well as employing a good performing design for PCM confinement. Incorporating fins to extend the heat exchanging area between the PCM and the in-charge heat-transfer fluid (HTF), is often recognized as the most common means for alleviating the low thermal response rates in TES systems (Mahdi & Nsofor, 2018b; Ghalambaz *et al.*, 2021a). Fin arrays, when properly structured and applied, have the potential to provide a high enhancement density while conserving the material usage and compactness of the system. Therefore, optimizing the layout of fins in thermal energy systems, including their size, placement, and material selection, has become a core concern for researchers in the field of thermal energy systems (Abdulateef *et al.*, 2018a; Sadeghianjahromi & Wang, 2021). Gradient-tree shaped (Yu *et al.*, 2020; Huang *et al.*, 2022) and fractal-tree-shaped fins (Zhang *et al.*, 2020; Huang & Liu, 2021) are among the recently suggested configurations due to their good enhancement capacity per the TES unit's volume. This study is dedicated to evaluating the potential of dimple-shaped fins as another new configuration for

improving the melting/charging performance of PCM-based storage systems.

The potential of extended fins for improving the thermal response of PCMs has been a topic of interest to several experimental and computational investigations over the past three decades. Lacroix (1993) reported that the inclusion of circular fins has a larger impact on the performance of shell-and-tube TES systems at moderate inlet temperatures ($\Delta T \geq 5$ K) and lower HTF flow rates ($m \leq 0.015$ kg s^{-1}). Velraj *et al.* (1997) showed that employing V-shaped fins in cylindrical TES systems can save the solidification time by about [1/(number of fins)]. Sciacovelli *et al.* (2015) revealed that employing Y-shaped fins can boost the solidification rate of PCM by 24%, and reported that larger Y-shaped fin angles are beneficial for short-duration operation while smaller Y-shaped fin angles are beneficial for long-duration operation. Abdulateef *et al.* (2018b) showed that using triangular fins results in a 15% quicker melting rate than using longitudinal fins in a triplex-tube storage unit. Mahdi and Nsofor (2017, 2018b) revealed that using fins alone in PCM composites outperforms using nanoparticles alone or a fin-nanoparticle combination within the same volume limitations of the enhancing additives. Ghalambaz *et al.* (2021b) reported that applying twisted fins may result in a 36% faster heat storage rate when compared to using longitudinal fins within the same PCM mass usage when compared to using longitudinal fins.

A key challenging problem that arises in applying fins is that their fixed, solid structure imposes too many flow-resistant forces that impact the beneficial contribution of natural convection during the melting phase of the heat-storage process in PCM systems. The application of non-uniform fin layouts to form better uniform melting at the different parts of the PCM domain has been proposed as a solution to overcome this problem. An attempt at this was initiated by Mahdi and Nsofor (2018a) who suggested employing non-uniform fin lengths at the different parts in the PCM domain to balance between the inhibition of natural convection and the augmentation of heat conduction due to the introduction of fins. Singh *et al.* (2019) proposed the use of non-uniform annular fins with a gradual reduction in the fin height in the vertical direction to further promote the enhancement potential of annular fins during the charging mode. Yang *et al.* (2020) tested various conditions for fin pitch and positions in a non-uniform pattern and reveal that proper shifting of fins down with the use of non-uniform fin lengths can effectively improve the melting homogeneity in vertical storage systems. Tang *et al.* (2021) indicated that applying non-uniform fin designs with fin lengths somewhat less than the shell radius and fins more concentrated in the bottom area of the PCM domain may significantly enhance the storage performance of latent TES systems.

The literature survey above reveals that there have been ongoing efforts to provide effective fin designs for superior performance enhancement in PCM-based storage systems. Consistent with these efforts, more investigations are required to test new fin configurations along with optimizing their geometric parameters, such as their fin dimensions, locations, and distributions, toward better enhancement potentials. In this view, the primary objective of this study was set to evaluate the capability of dimple-shaped fins as a new fin configuration to improve the thermal PCM characteristics during the energy charging and discharging modes in a shell-and-tube containment type. The second objective was to optimize the size, arrangement, and placement of dimple fin arrays over a range of thermal and flow conditions in the PCM containment design. Dimple-shaped fins are a novel fin shape that has been rarely discussed in the literature, especially for latent heat

Table 1: Geometric parameter specifications of different dimple-shaped fin configurations.
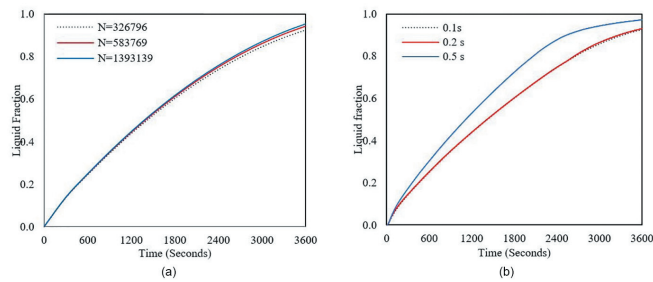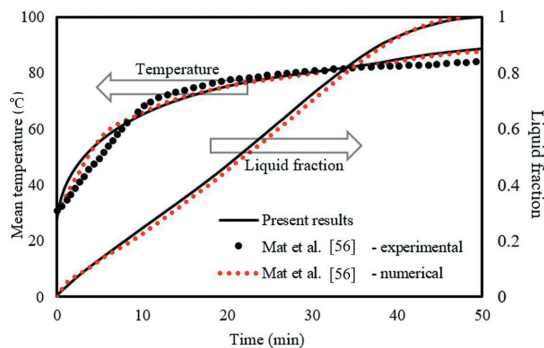
Cases	Number of fins	Number of fins in each section	Number of arrays	Radius of fins	Volume of fins
Case 1 (base case)					
Case 2	8	2	4	4	2144.66
Case 3	16	4	4	3.18	2144.66
Case 4	24	6	4	2.77	2144.66
Case 5	32	8	4	2.52	2144.66

Table 2: Thermofluidic property values of RT35 PCM (Rubitherm GmbH, n.d.).

Property	μ (N s m^{-2})	β (K^{-1})	C_p (kJ kg^{-1} K^{-1})	k (W m^{-1} K^{-1})	ρ (kg m^{-3})	L_f (kJ kg^{-1})	T_L (°C)	T_s (°C)
Values	0.023	0.0006	2.0	0.2	815	170	35	29

Table 3: The characteristics of the grids used for mesh independence analysis.

Grid number	Time-step size	Node number (N)	Cell number
1	0.2	326 796	1 319 025
2	0.1	583 769	1 972 730
3	0.5	1 393 139	5 832 898

Figure 2: The effect of (a) grid number and (b) time-step size on the liquid fraction variation for Case 5 with 32 fins.

Figure 3: Comparison of the simulation model's temperature and liquid-fraction evolution predictions to those of Mat *et al.* (2013).

Figure 4: Schematic of vertical shell-tube TES system with different arrangements of dimple fins.

the heat penetration in the PCM domain from the heat source is lower in the system equipped with dimple-shaped fins. So, this study aims to study the performance of dimple-shaped fins to find out how effective dimple-shaped fins can be in the thermal management of PCM-based systems. Therefore, a numerical model was developed using the computational-fluid-dynamic package (ANSYS FLUENT) in connection with developing specific codes in MATLAB for evaluating the involved performance indices such as liquid-fraction evolution and temperature distribution. A three-dimensional (3D) computational model based on finite-volume discretization was developed considering the effects of natural convection in PCM and the temperature-dependent thermal properties of PCM. To the best of the authors' knowledge, no previous research has discussed the impact of dimple fins on the enhancement of PCM thermal response in latent TES systems. The study would provide, in this regard, a distinct benchmark for designing fast-responsive PCM-based storage systems over a range of temperature and flow conditions that are able to suit a wide range of engineering applications.

2. System Description

In this study, a sequence of 3D simulations was carried out to assess the potential of dimple-shaped fins to facilitate faster energy storage rates during the melting of PCM in a double-tube containment system. The double-tube heat exchanger was modeled vertically, and the PCM was located in the outer tube, while the HTF was passed through the inner tube to melt the PCM and store the thermal energy. Figure 1 illustrates the schematic of the
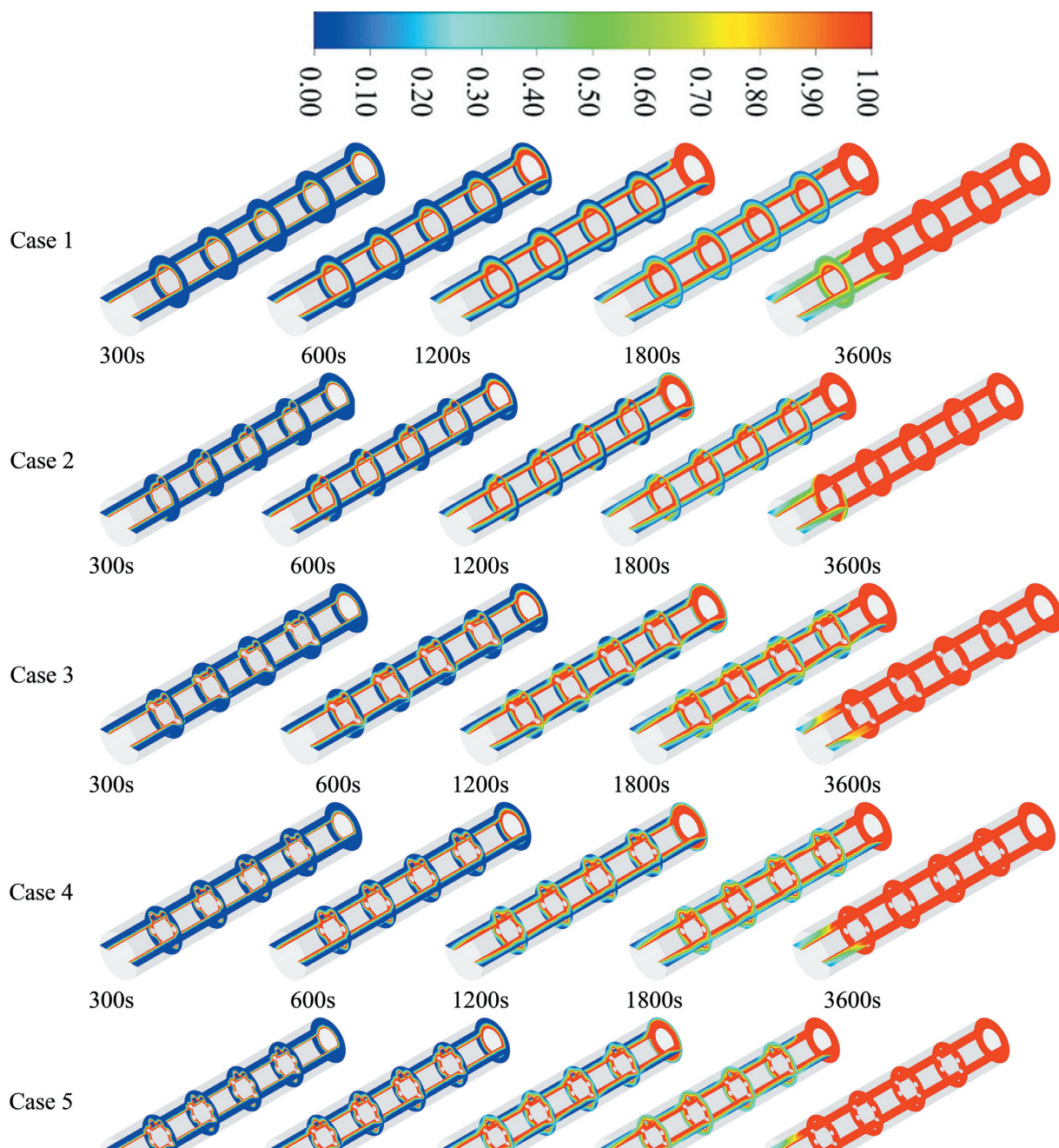
storage and phase change problems. Due to the shape of the dimples, which are hemispherical, the fins do not prevent the circulation of liquid PCM in the domain by natural convection, which is one of the disadvantages of using fins in the PCM-based thermal storage systems. However, due to the lower height of dimple-shaped fins compared with that of the conventional form of fins,

Figure 5: The contours of liquid-fraction evolution for different arrangements of dimple fins at distinct durations of the melting evolution.

system, including the boundary conditions and the dimensions for the system with 32 dimple fins. The length of the tube is 250 mm, while the diameters of the inner and outer tubes are 20 and 40 mm, respectively. The thickness of the inner tube is also considered to be 2 mm. These dimensions are chosen based on different studies in the literature (Shahsavar *et al.*, 2020). The inlet is assigned a uniform temperature and velocity, while the outlet is assigned a pressure outlet condition. A no-slip boundary condition is also used for the walls. The outer tube and sides of the PCM domain are also insulated to prevent heat loss to the environment.

There are five main scenarios investigated in this research to reach the optimum fin array: (i) determining the optimum number of dimple fins to be used, (ii) determining where to locate the first

fin section, (iii) determining the optimum fin spacing for the best case, (iv) determining the optimum fin spacing based on the aromatic algorithm, and (v) employing a staggered fin arrangement to further improve the melting performance. It should be noted that the schematics of the proposed cases in different scenarios are displayed separately in the discussion section in the related part to better understand the geometry of different cases. Different numbers and diameters are studied for the dimple-shaped fins. Table 1 shows the dimensions of different sizes of the dimple-shaped fins. In all scenarios, the total volume of fins is kept constant at 2144.66 mm³ to enable meaningful comparisons of storage performance indices to be made across the board. A total of three key indicators were selected to assess the overall performance of the system. This includes the timewise melting-front
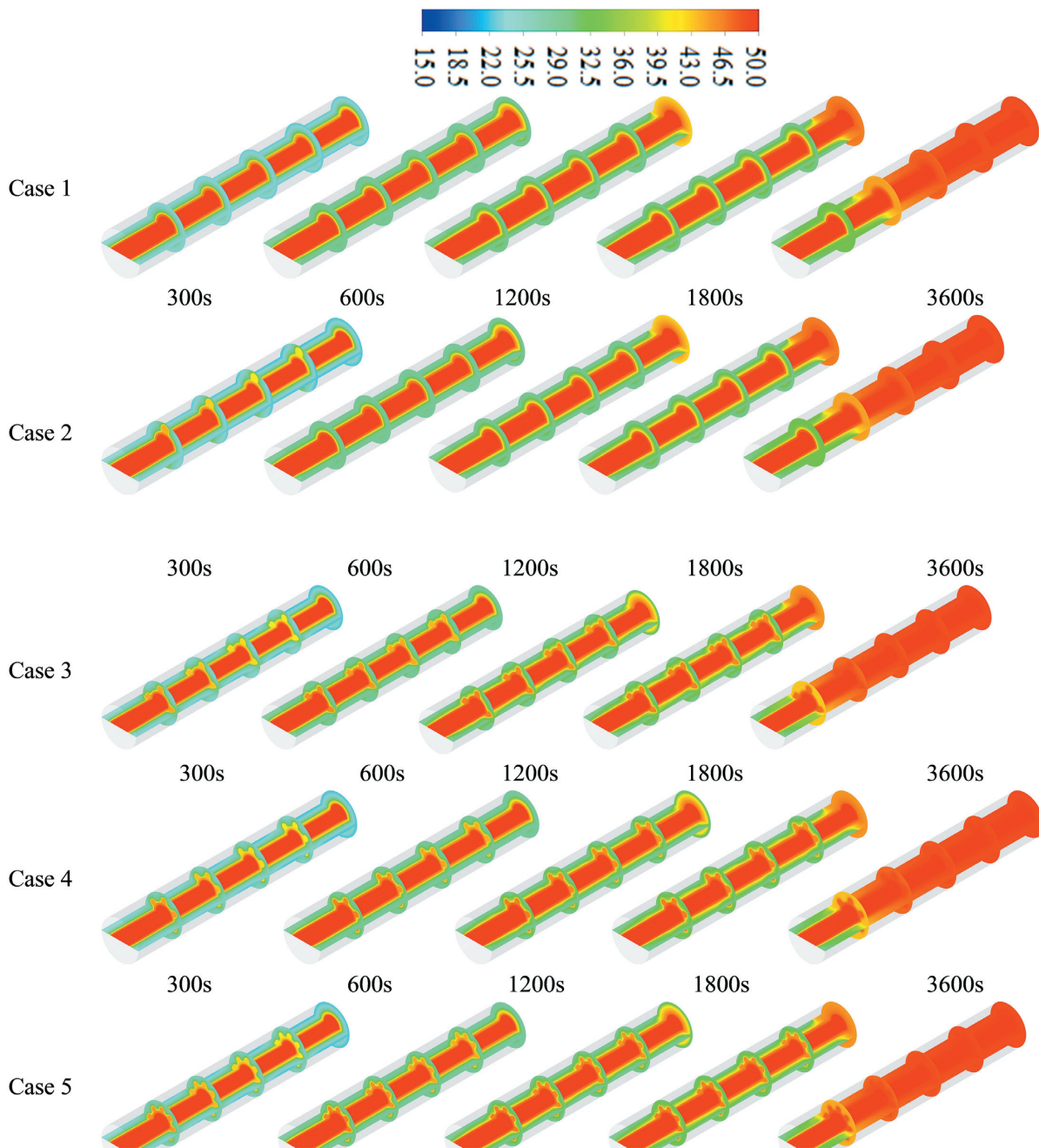
Figure 6: The contours of isotherm distribution for different arrangements of dimple fins at distinct durations of the melting evolution.
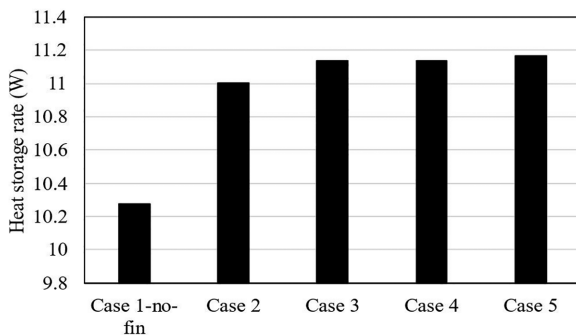

Figure 7: The overall heat storage rates for different arrangements of dimple fins.

evolution, timewise isotherm distribution, and nominal energy storage rates.

To ensure that PCM melting begins from a liquid state, it is assumed that each scenario to achieve complete melting begins when the PCM at initial temperature ($T_{int} = 15°C$) is lower than the PCM solidus temperature ($T_s = 29°C$). In the meanwhile, the HTF (water) is circulating at a lower temperature (i.e., 50°C) to provide the desired heating demand. This enables the development of melting layers next to thermally active partitions in the domain so that the PCM layers closest to the heating wall cause the completion of melting to occur sooner than the other PCM layers. In this regard, the incorporation of dimple fins would allow for quicker melting rates in the wall-nearby PCM layers by higher heat transfer to the PCM domain resulting in an improved overall energy
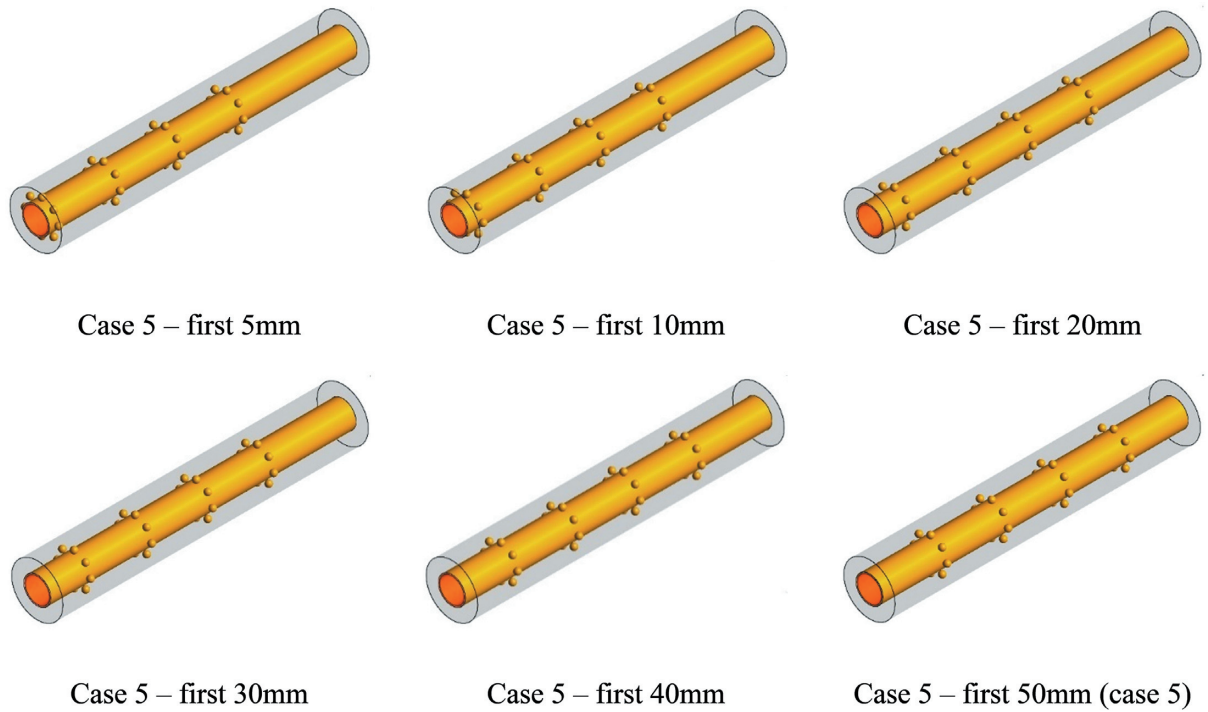
Figure 8: Schematic of dimple fins of Case 5 with different spacings for the first fin section.

storage process across the whole TES unit. RT35 was employed as the PCM inside the dimple-shaped fin double-pipe heat exchanger in this study and Table 2 shows the properties of the RT35 PCM.

3. Mathematical Modelling

The enthalpy–porosity approach is incorporated to estimate the thermofluidic behavior of PCM during the phase change process. The following set of assumptions is adopted to enable the numerical solution and make the mathematical modeling more straightforward (Li *et al.*, 2019):

(i) Buoyancy-driven of liquid PCM flow is laminar, transient, and Newtonian.
(ii) PCM has constant thermofluidic properties except for density.
(iii) Boussinesq model is employed to predict density variation.
(iv) Volume change of PCM during phase transition is ignorable.
(v) Viscous dissipation is neglected due to the law velocities of liquid PCM.

Considering the above assumptions, the standard governing equations of mass, momentum, and energy are formulated as follows (Talebizadehsardari *et al.*, 2021b):

$$\frac{\partial \rho}{\partial t} + \nabla.\rho \vec{V} = 0, \tag{1}$$

$$\rho \frac{\partial \vec{V}}{\partial t} + \rho \left(\vec{V}.\nabla \right) \vec{V} = -\nabla P + \mu \left(\nabla^2 \vec{V} \right) - A_m \frac{(1-\lambda)^2}{\lambda^3 + 0.001} \vec{V}$$
$$- \rho_{\text{ref}} \beta \left(T - T_{\text{ref}} \right) \vec{g}, \tag{2}$$

$$\frac{\rho C_p \partial T}{\partial t} + \nabla \left(\rho C_p \vec{V} T \right) = - \left[\frac{\partial \rho \lambda L_f}{\partial t} + \nabla \left(\rho \vec{V} \lambda L_f \right) \right] + \nabla \left(k \nabla T \right). \tag{3}$$

The momentum sink for the phase change in the mushy zone is represented as the third term on the right-hand side of Equation

(2). The volume expansion due to change in the PCM from solid to liquid state is neglected in this research, and A_m was considered 10^{-5} (Pan *et al.*, 2018; Fadl & Eames, 2019). For the water flow simulation in the inner tube, similar governing equations are employed, ignoring the body forces and phase change equation. λ is introduced as (Brent *et al.*, 1988):

$$\lambda = \frac{\Delta H}{L_f} = \begin{cases} 0 & if\,T < T_S \\ \frac{(T - T_S)}{(T_L - T_S)} & if\,T_S < T < T_L \\ 1 & if\,T > T_L \end{cases}. \tag{4}$$

A detailed description of the mathematical model can be found in the authors' previous work (Mahmoud *et al.*, 2021; Sun *et al.*, 2021). The total enthalpy (H) is achieved as:

$$H = \Delta H + h, \tag{5}$$

where

$$h = \int_{T_{\text{ref}}}^{T} C_p dT + h_{\text{ref}}. \tag{6}$$

The heat charging rate $\dot{Q}$ is introduced as:

$$\dot{Q} = \frac{Q}{t_m} = \frac{m \left(\int_S C_p dT + L_f + \int_L C_p dT \right)}{t_m}, \tag{7}$$

where t_m is the melting time and *m* is the mass of PCM.

4. Numerical Modelling and Validation

The simulation is performed in ANSYS FLUENT software employing the QUICK scheme for the diffusion fluxes and convection and PRESTO scheme for the pressure correction equation. The convergence criteria of 10^{-6} is also assumed. Different mesh elements and time-step sizes are evaluated so that the results are unconditional to grid density and time-step.
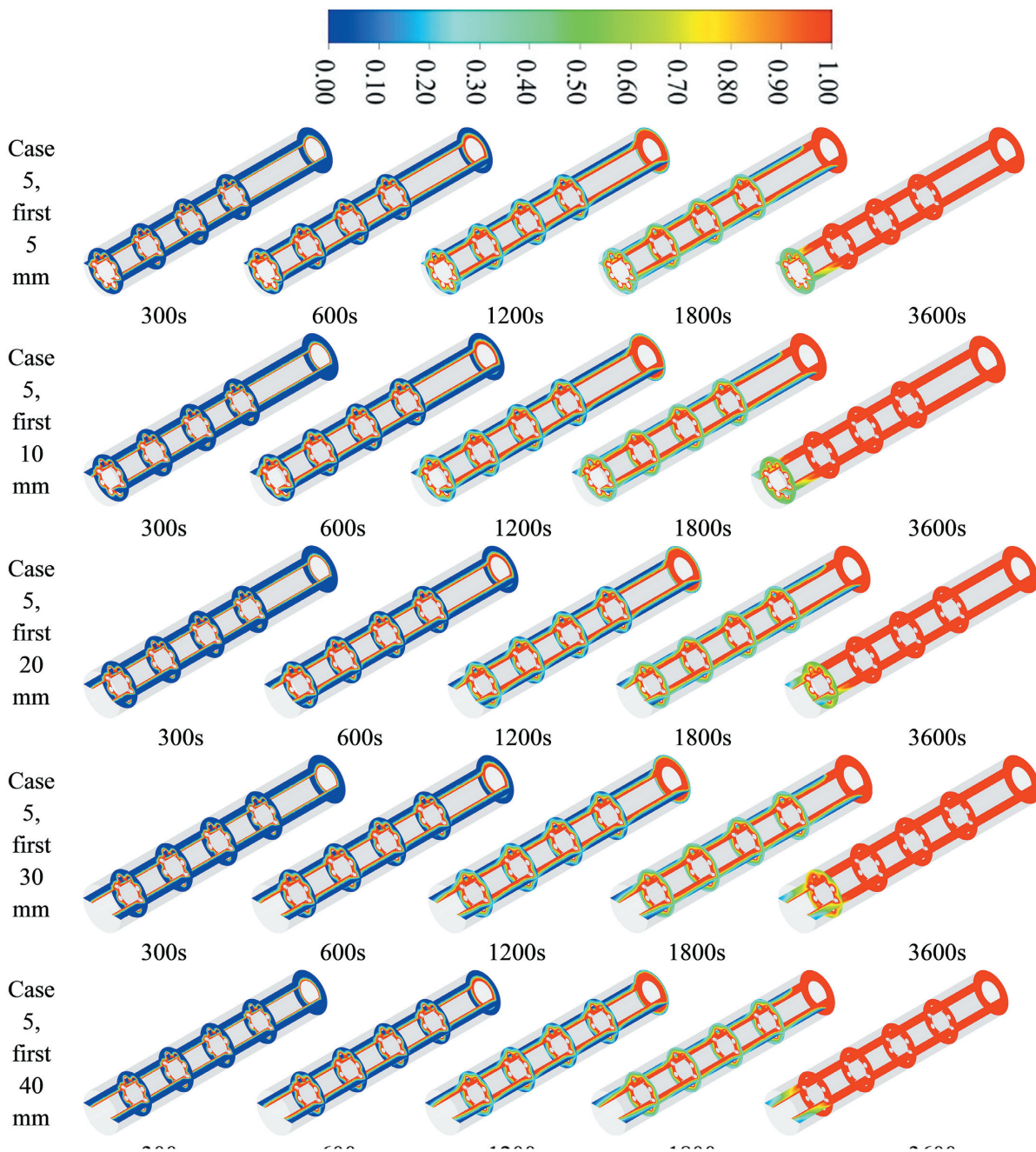
Figure 9: The contours of liquid-fraction evolution for Case 5 with different spacings of the first fin section at distinct melting durations.

4.1 Mesh independence analysis

Mesh with node number of $N = 326\,796$, $583\,769$, and $1\,393\,139$ are generated for the mesh independence analysis for Case 5 with 32 dimple-shaped fins with uniform distribution. The mesh with the node number of $583\,769$ is selected since the results are almost identical to those of $1\,393\,139$ nodes. The size of the mesh and the cell numbers for different grids are listed in Table 3.

For the selected mesh, three different time-step sizes of 0.1, 0.2, and 0.5 s are investigated and the results are illustrated in Fig. 2a. The results show that the variations of liquid fraction for the time-step sizes of 0.1, 0.2, and 0.5 s are almost similar in Fig. 2b, and thus the time-step size of 0.2 s is selected for further analysis. It should

be noted that Case 5 with 32 dimple fins which is introduced later in the discussion section is used for the mesh independence and time-step size analysis.

4.2 Model validation

To verify the accuracy of the numerical scheme applied in the present study, the numerical results of the present research are validated against those of Mat *et al.* (2013). The same boundary conditions and performance parameters of the reference system are applied in the present model. Mat *et al.* (2013) conducted a set of numerical and experimental investigations to explore the melting performance of a PCM (RT82) in a double-tube TES system. The objective of their research was to evaluate the impacts of adding
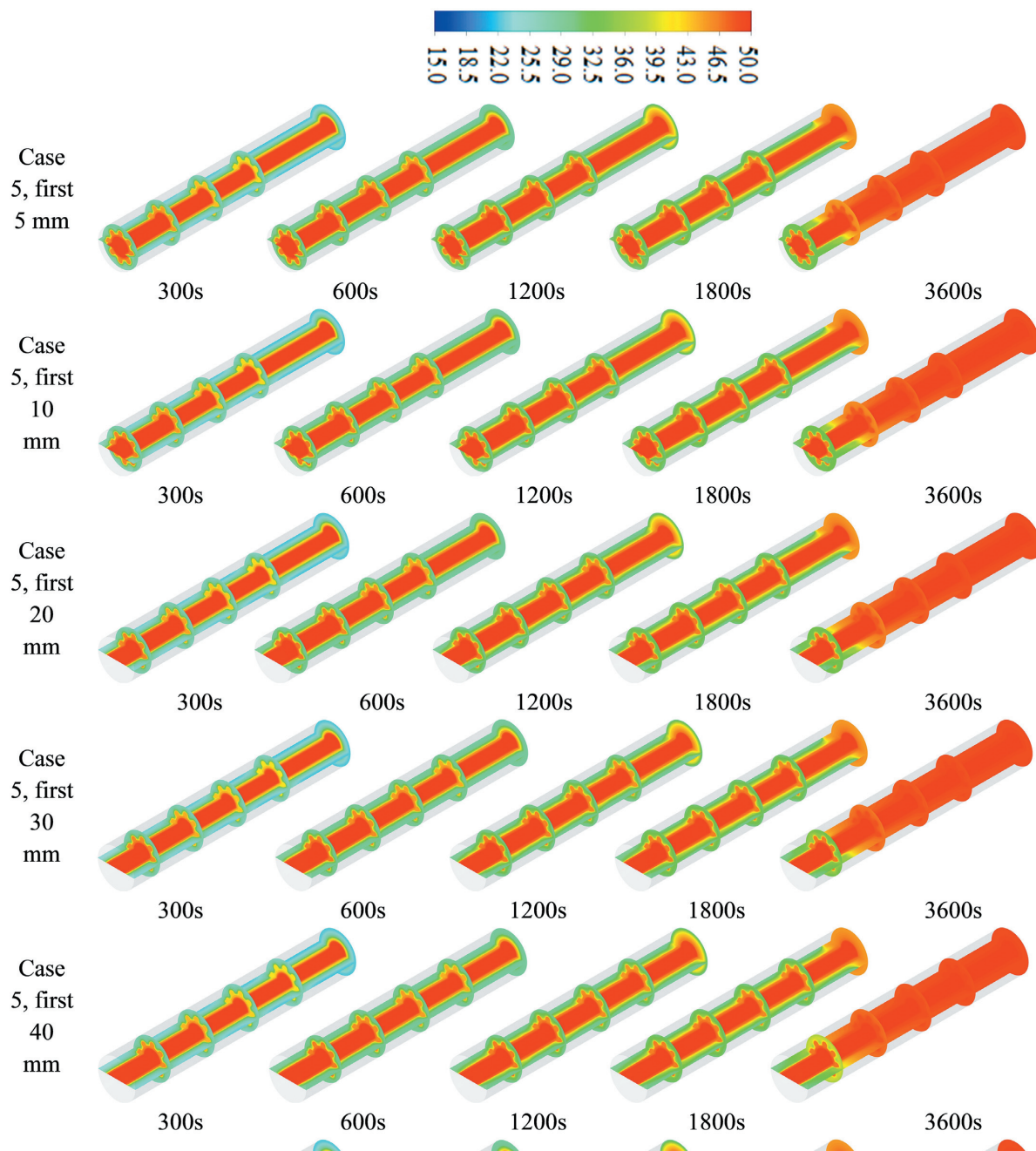
Figure 10: The contours of isotherm distribution for Case 5 with different spacings of the first fin section at distinct melting durations.
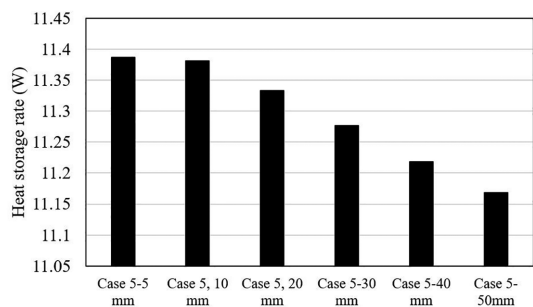

Figure 11: The overall heat storage rates for Case 5 with different spacings of the first fin section.

staggered fins to the exterior and interior walls of the PCM shell. At the beginning of tests, all PCM was at solid phase so that the temperature was initially set to 27°C. During the tests, the temperature of HTF was kept at 90°C so as to the internally finned tubes maintain a constant temperature (T_{wall} = 90°C) as the boundary condition. The data for the average PCM temperature and liquid fraction from the present study are compared to the numerical and experimental findings reported by Mat *et al.* (2013) as shown in Fig. 3. The statistical comparison gave a maximum percentage error of 1.4%. Thus, the present model can be adopted for exploring the thermal characteristics of the PCM-based system for further analysis.
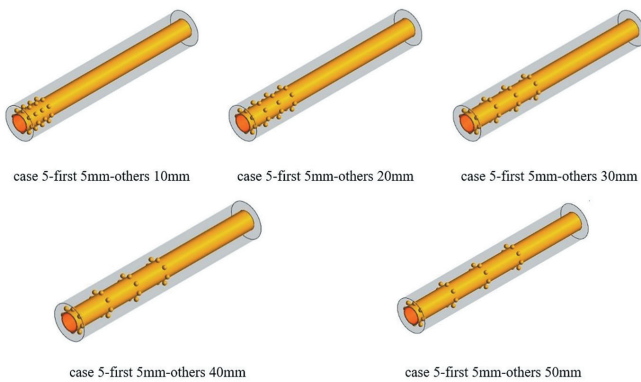
Figure 12: Schematic of dimple fins of Case 5 with 5 mm spacing of the first fin section and different spacings of other fin sections.

5. Results and Discussion

5.1 Impact of applying different numbers of dimple fins

A parametric study was carried out using data from the simulation cases under the consideration to assess the thermal performance of various arrays of dimple fins with different numbers of 0, 8, 16, 24, and 32 fins as shown in Fig. 4 during the PCM melting mode.

Figure 5 depicts the liquid-fraction contours, as well as the melting fronts (in light green), for the dimple fin arrays considered in this study throughout five melting durations: 300, 600, 1200, 1800, and 3600 s. The melting fronts (in light green) are shown for the five cases considered in this section. Early durations (i.e., 300–1200 s) witness the formation of light-green melting fronts as characterized by the appearance of homogenous circles, which are comparable in the vertical direction between the different cases of dimple fins. It can be observed from the figure that employing a larger number of dimple fins, particularly at high numbers such as 24 and 32 fins, causes an increase in the size of melting layers (red regions) between and around the fin zones as a result of the introduction of dimple fins. This is due to the fact that only thin liquid layers are capable of forming during this time, and as a result, the melting fronts are seldom seen to be moving apart during this period. The forms of melting fronts get progressively distorted as the time approaches the halfway time point ($t = 1800$s). This is especially observable in cases where there are a higher number of fins such as that in Cases 4 and 5. The reason would be the faster heat storage rates at the heating walls, which continue to increase as time goes on. When looking at the same contour maps, it can be seen that the size of the melting layers (red zones) seems to be increasing gradually toward the bottom during the course of the 3600s ultimate duration. Due to the fact that convection is more important in the upper parts of the domain than it is in the lower parts would be the explanation for such a behavior of liquid PCM. While dimple fins are advantageous in that they allow greater heat dispersion to PCM portions that are located far away from thermally active walls, they also benefit from the fact that they cause the melting layers to increase in size more rapidly throughout the latter duration of the process (i.e., $t = 3600$s). Natural convection has a higher role in the presence of dimple fins since the distortion of the melting front increases as a result of the increased distortion during final melting durations. This is due to the fact that dimple fins have their unique flow-aiding structure, which makes them more advantageous in terms of encouraging heat transfer through natural convection.

Figure 6 depicts the isotherm evolution for the five cases explored in this section of 0, 8, 16, 24, and 32 dimple fins during the melting periods of 300, 600, 1200, 1800, and 3600s. The radiuses of the fins are 4, 3.18, 2.77, and 2.52 mm, respectively, for the system with the fins' numbers of 8, 16, 24, and 32. An initial insight at the isotherm maps indicates that the high-temperature isotherms at 35°C (the red areas) are the leading band in all studied cases at early durations. This may be ascribed to the fact that the majority of PCM remains in the solid-state during these periods. As can be seen from the figure, melting has limited influence on the isotherm distribution during this duration, and the isotherms between and within a short distance of the fin neighborhood seem to be almost similar in terms of their behavior and appearance. During the later durations, the isotherms with higher temperatures above 35°C (turquoise areas) begin to progressively reduce across the domain, particularly in the cases with a larger number of fins. This is notably true in the cases with fins at times ($t = 1200$–1800s). Because of the increased heating effect of the HTF on PCM melting behavior during this period, the melting layer grows in size and finally occupies the whole domain. Aside from that, the presence of dimple fins helps to improve the effectiveness of heat transfer from the PCM to the HTF by allowing for more effective communication between the PCM layers that are further away from thermally active walls and the HTF in charge. In comparison to the base case of no fins, there is a stronger discoloration of isotherms at high temperatures in the cases with fins throughout the final period of the testing (i.e., $t = 3600$s) when moving down in the domain. As compared to the role of conduction, convection heat transfer has a more noticeable role in the cases of fins, particularly in the upper portion of the domain. The isotherms seem to have become more uniform in their shape and behavior during the course of the final periods. Due to the good role played by convection in certain localities, the melting process is finished much quicker in the upper parts than it would be in other locations. By virtue of their spherical configuration, the presence of dimple fins leads to a more dominant role in heat convection during melting. This would reinforce the evasiveness of natural convection and substantially assists the overall heat transfer process.

The values of the overall heat storage rate for all cases investigated in this section, i.e., Cases 1, 2, 3, 4, and 5, with dimple fins of 0, 8, 16, 24, and 32 correspondingly, are summarized in Fig. 7. The data from the figure indicate that heat storage rates were recorded at 10.23, 11.00, 11.12, 11.14, and 11.18 W for Cases 1–5, respectively. These results imply that increasing the number of dimple fins from 0 to 8, 16, 20, and 24 fins would result in heat storage rates by about 7.1, 8.4, 8.4, and 8.7% faster than they would be otherwise.

5.2 Impact of varying the spacing of the first fin section

Following the determination of the optimal case of fin number (i.e., Case 5), this part examines the influence of fin placement to determine where to locate the first fin section for the better melting performance of PCM. As shown in Fig. 8, six different spacings (5, 10, 20, 30, 40, and 50 mm) for the first fin section with a constant spacing for the other fin sections were tested by studying the contour lines of liquid fraction and PCM temperature in addition to the heat storage rates.

Figure 9 shows the liquid-fraction contours as well as the melting fronts (in light green) for the dimple fin arrays considered in this section across five melting times: 300, 600, 1200, 1800, and
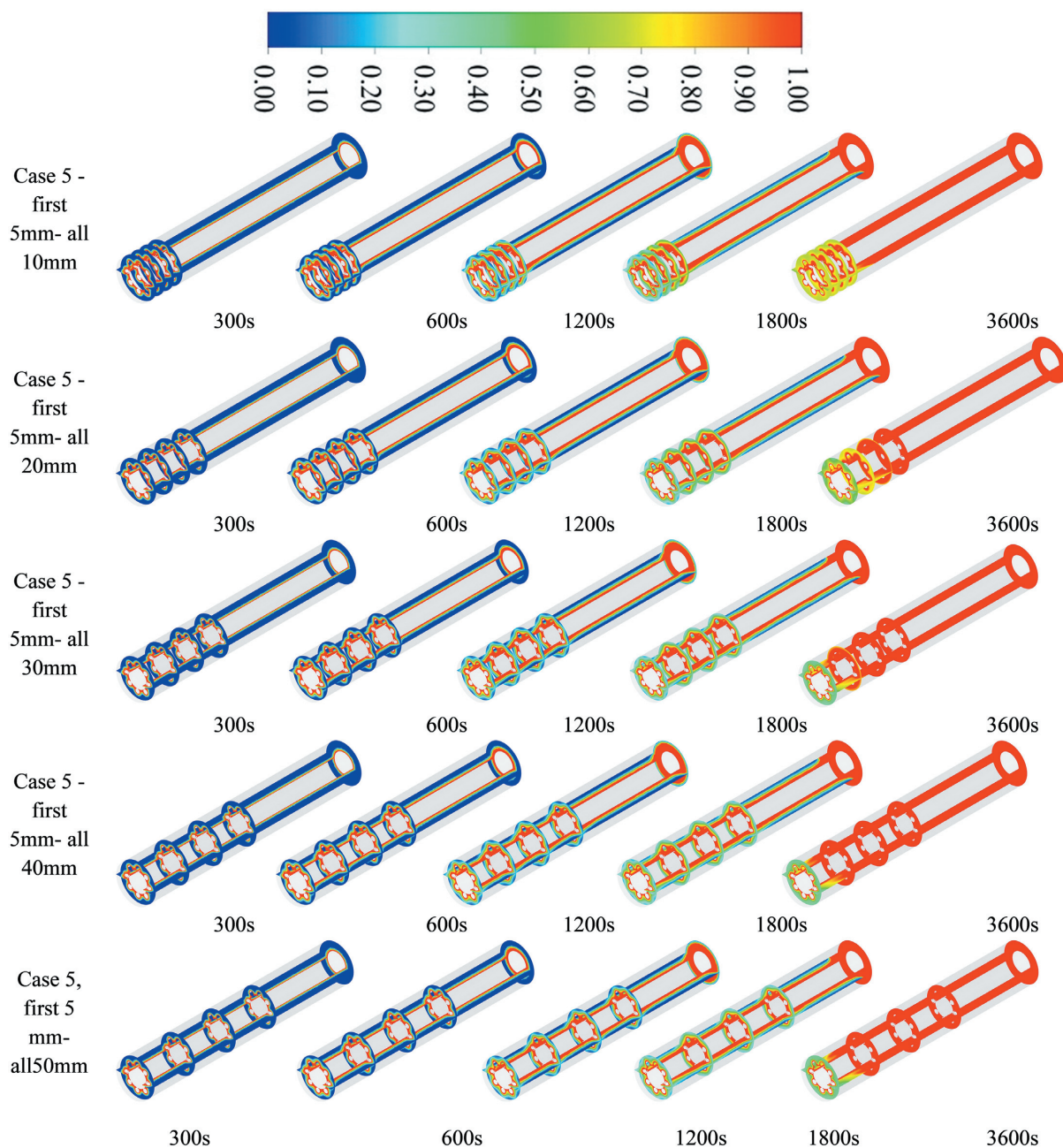
Figure 13: The timewise contours of liquid-fraction evolution for Case 5 with 5 mm spacing for the first fin section and different spacings for other fin sections.

3600 s. The figure shows that employing lower spacings for the first fin section, especially at smaller values like 5 and 10 mm, serves for larger melting layers (red areas) between and around the fin zones to produce during the course of the 3600s. The contour maps in Fig. 9 show that the size of the melting layers (red zones) seems to be decreasing steadily toward the bottom, especially during the final duration. This behavior of liquid PCM might be explained by the fact that convection is more prominent in the regions between the fins. By reducing the spacing of the initial fin section, more room is made available for natural convective currents to pass through, allowing for higher heat transmission for PCM parts located near the HTF entrance. As a result, lowering the spacing of the first fin section provides a better flow-aiding structure for dimple fin arrays, making them more beneficial in terms of boosting enhanced heat transfer via natural convection.

Figure 10 depicts the isotherm evolution for the six cases explored in this section of a fins' spacing of 5, 10, 20, 30, 40, and 50 mm for the first fin section during the melting periods of 300, 600, 1200, 1800, and 3600s. An initial insight at the isotherm maps reveals that isotherms with higher temperatures over 35°C (turquoise patches) begin to steadily decline throughout the domain, especially when smaller spacings of 5 and 10 mm are used. The melting layer expands in size and eventually covers the whole domain because of the increasing heating influence on PCM melting behavior during the later period ($t > 1800$ s). This would be attributable to the fact that decreasing the distance between the entrance and the first fin section improves the efficacy of natural convection heat transfer by allowing for more efficient buoyancy-driven flows to be generated between the fin zones. Throughout the final period (i.e., $t = 3600$ s), there is a greater discoloration of
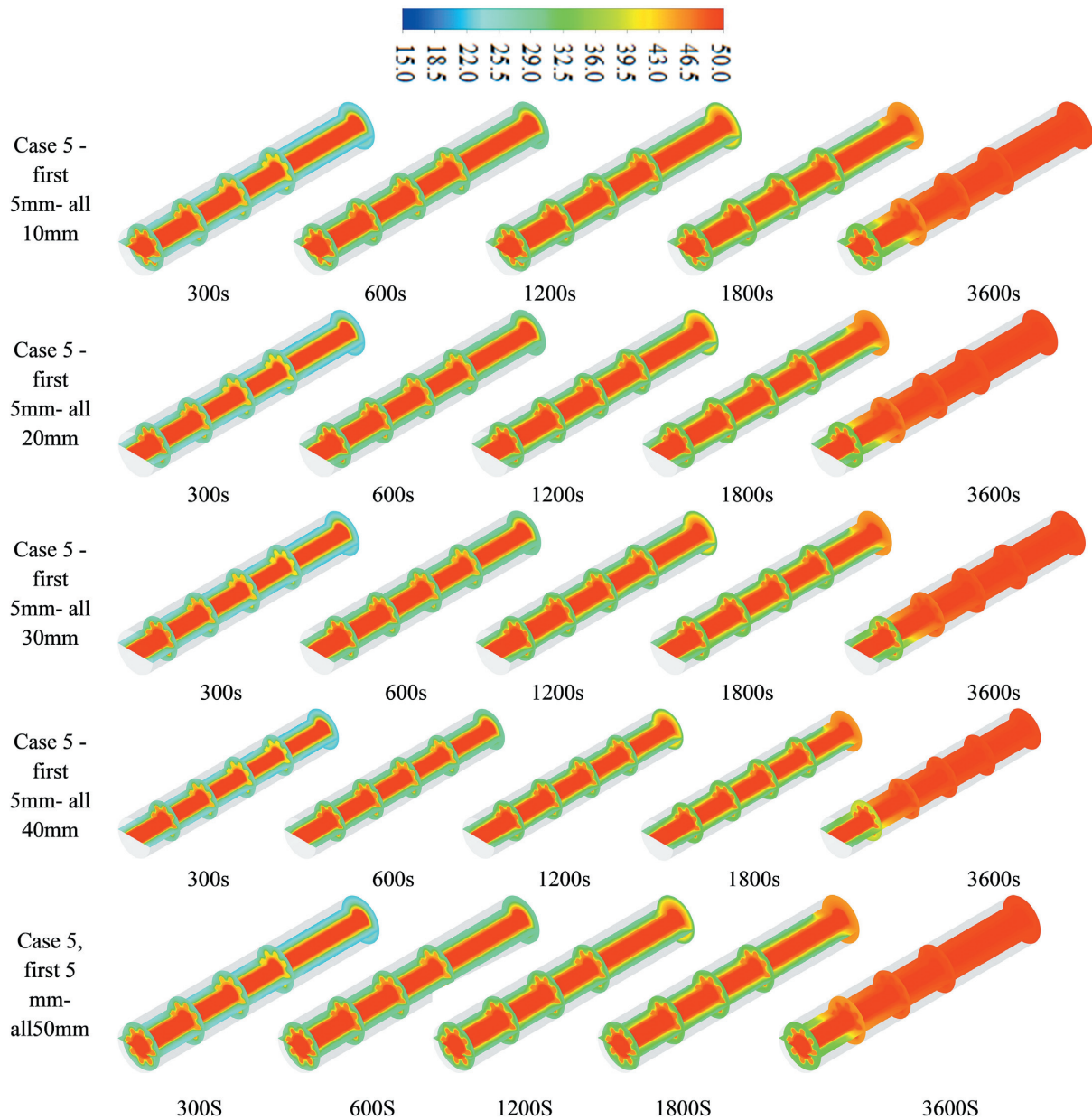
Figure 14: The timewise isotherm distribution for Case 5 with 5 mm spacing for the first fin section and different spacings for other fin sections.
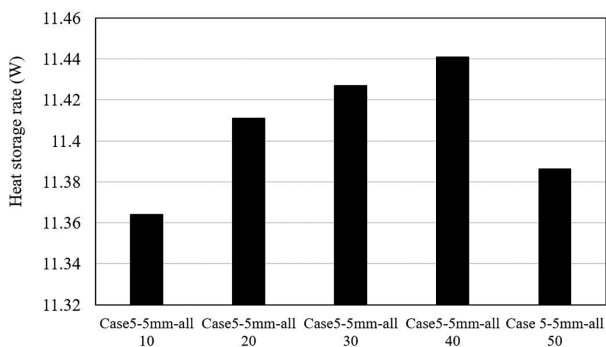

Figure 15: The overall heat storage rates for Case 5 with 5 mm spacing for the first fin section and different spacings for other fin sections.

isotherms in cases with wider spacings of the first fin section, such as that in the base case of 50 mm. This isotherm discoloration indicates that convection contribution is more visible than that by conduction at lower fin spacings, especially in the top region of the domain. Therefore, isotherms seem to have grown more uniform in shape and behavior over the final periods, in particular, at lower spacings of the first fin section owing to the good role played by convection in these localities.

The values of the overall heat storage rate for all cases explored in this section, i.e., Case 5 with a spacing of (5, 10, 20, 30, 40, and 50 mm) for the first fin section, are summarized in Fig. 11. According to the obtained data, heat storage rates were 11.39, 11.33, 11.28, 11.21, and 11.16 W for 5–50 mm spacings of the first fin section, respectively. These results imply that reducing the spacing for the first fin section from 50 mm to 40, 30, 20, 10, and 5 mm would
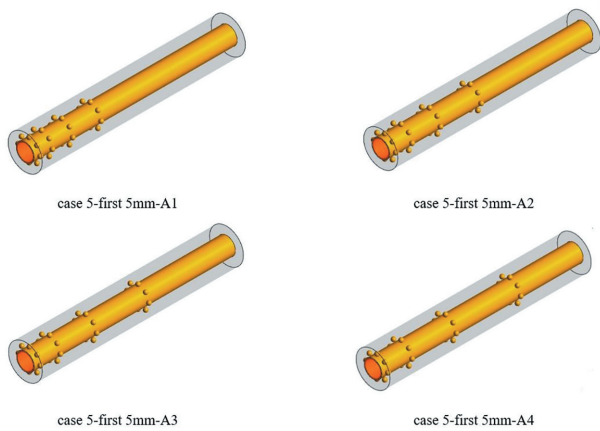
Figure 16: Schematic of dimple fins of Case 5 with fin spacings being optimized based on the aromatic algorithm.

result in faster heat storage rates by about 0.5, 1.0, 8.4, and 1.4, 2.0% than they would be otherwise.

5.3 Impact of varying the spacing between the different fin sections

After identifying the best spacing for the first fin section (i.e., Case 5 first-5 mm), this part investigates the influence of fin placement to determine where the fin sections other than the first fin section should be located for better enhancement rates of melting. As shown in Fig. 12, five various spacings (10, 20, 30, 40, and 50 mm) for the different fin sections were evaluated in terms of the contour lines of liquid fraction and temperature, as well as heat storage rates.

Figure 13 illustrates that increasing the spacing between the fin sections from 10 to 40 mm allows for greater melting layers (red zones) to form between and around the fin sections during the course of melting when using higher spacings. The figure shows that the size of the melting layers (red zones) appears to be reducing steadily toward the bottom of the domain, particularly throughout the final durations of the test. This behavior of liquid PCM may be explained by the fact that convection is more prominent in areas where fin spacings are larger. When the spacings between fin sections are increased, more space is made available for natural convective currents to pass through, resulting in higher heat diffusions across the PCM layers involved. Increasing the spacing between dimple fin sections, as a result, drives a better flow-aiding structure for dimple fin arrays, making them more advantageous in terms of enhancing the heat transfer rates via natural convection.

Figure 14 displays the isotherm development for the five cases investigated in this section with spacings of (10, 20, 30, 40, and 50 mm) throughout the melting periods of 300, 600, 1200, 1800, and 3600 s. According to the isotherm maps of Fig. 14, the higher temperature isotherms (turquoise patches) continue to slowly fade away across the domain, especially when bigger spacings of 40 mm are employed. This would be due to the fact that increased distance between fin sections enhances the efficacy of natural convection by allowing for more efficient buoyancy-driven flows to be formed between the fin sections. Also, there is more discoloration of isotherms can be observed during the last melting periods in cases with larger spacings of fin sections, such as the

Table 4: The nominal distance values for fin sections in different cases based on the aromatic algorithm.

Cases	1st section position	2nd section position	3rd section position	4th section position
Case A1	5	20	45	80
Case A2	5	25	60	110
Case A3	5	30	75	140
Case A4	5	35	90	170

basic case with 40 mm between fin sections. This isotherm discoloration indicates that the contribution of convection is more noticeable than the contribution of conduction at larger fin spacings, which is particularly true in the top portion of the domain. As a result, the isotherms at wider fin spacings become more consistent in shape and behavior throughout the course of the last periods, owing to the important role played by convection in these locations.

The corresponding values of the heat storage rate for all cases explored in this section are summarized in Fig. 15. The obtained data shows that heat storage rates were 11.33, 11.41, 11.43, 11.45, and 11.38 W for 10, 20, 30, 40, and 50 mm spacings of the fin sections, respectively. This implies that increasing the spacing between fin sections from 10 mm to 20, 30, 40, and 50 mm would result in faster heat storage rates of about 0.7, 0.9, 1.2, and 0.5% than they would have been if the spacing is kept constant at 10 mm.

5.4 Impact of varying the fin spacing based on the aromatic algorithm

The effects of modifying the fin spacing between the various fin sections using the aromatic method are examined considering the optimal spacing for the first fin section (i.e., 5 mm), see Fig. 16. Table 4 lists the nominal distance values from the bottom for the four fin sections evaluated in each of the four Cases A1, A2, A3, and A4 considered in this section.

Figure 17 depicts the liquid-fraction evolution contours for the four cases explored in this section during the melting periods of the 300, 600, 1200, 1800, and 3600 s. Comparing the different cases in the figure shows that increasing the fin spacings according to the distances stated in Case A2 enables larger melting layers (red zones) to form between and around the fin sections. This behavior would be attributed to the fact that increasing the spacings between fin sections creates more area for natural convective currents to move through, resulting in larger heat diffusions across the PCM layers involved. Meanwhile, increasing the lengths between fin sections allows more PCM to settle between the fin sections, causing the melting to take longer in these zones to complete. As a result, there is a tradeoff between speeding the melting speed through natural convection and limiting the melting spread potential through the increased amount of PCM involved when bigger spacings between the fin sections are used. As shown in Fig. 17, the particular fin spacings of Case A2 drive the best flow-aiding structure for dimple fin arrays to provide the best melting enhancement via natural convection.

Figure 18 compares the isotherm distributions for the four Cases A1, A2, A3, and A4 examined in this section across melting intervals of 300, 600, 1200, 1800, and 3600 s. The top sections of the PCM domain constantly exhibit a remarkable isothermal discoloration in all cases tested, indicating a more dominating role
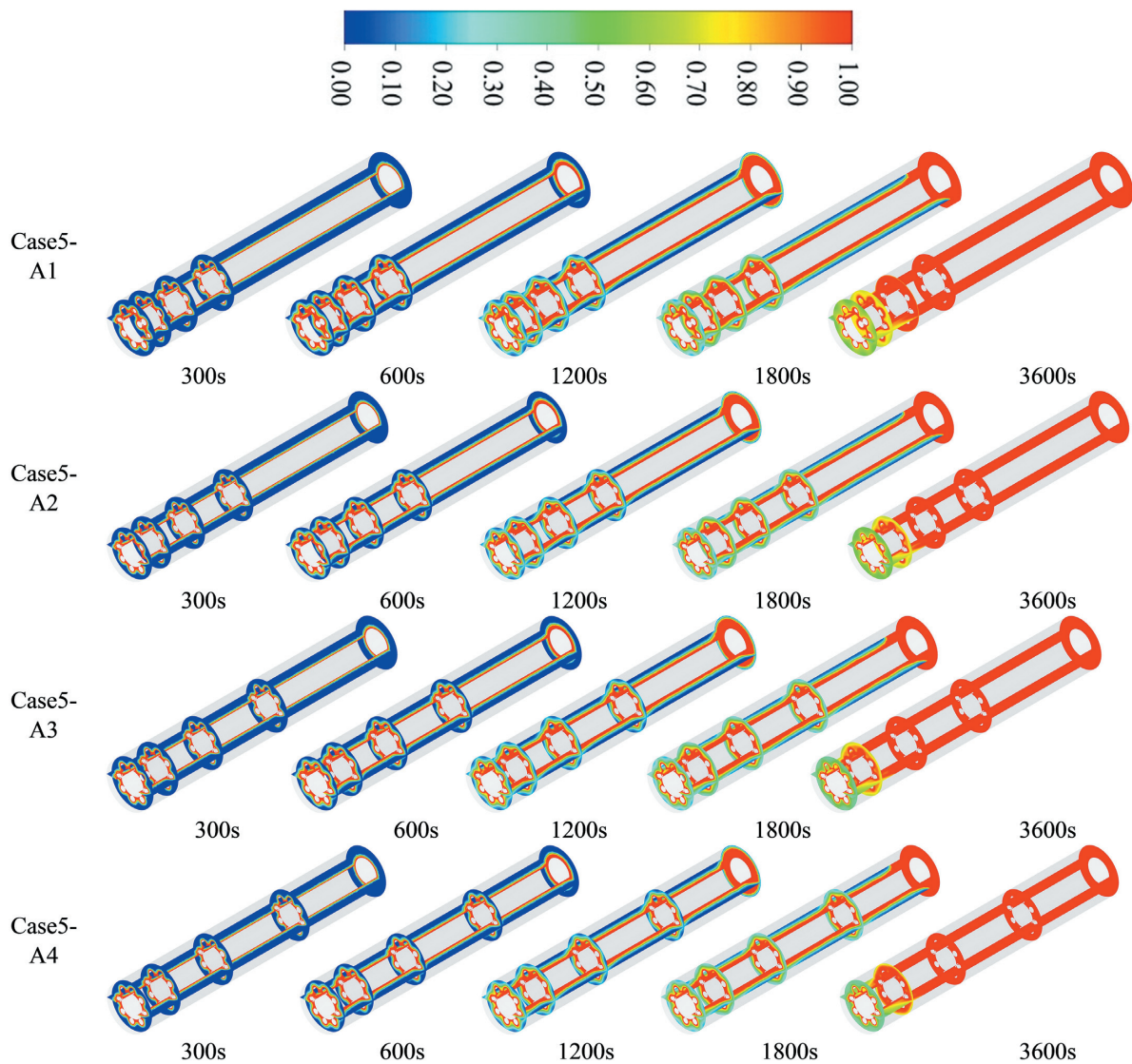
Figure 17: The timewise liquid-fraction evolution for Case 5 with fin spacings being optimized based on the aromatic algorithm.

of convection over that of conduction in these parts. Meanwhile, conduction dominates the bottom part of the domain, resulting in slight isothermal discoloration as can be seen during the final periods of melting. However, the optimal spacing of the fin sections according to the aromatic algorithm would further support the efficiency of natural convection by allowing for the formation of warmer PCM layers (red zones) throughout the melting duration. This is because the region contained between any two subsequent sections of dimple fins is typically impacted by the thermal impact of both fins. Thus, PCM regions with closer fins contribute more conduction but less convection. Figure 19 depicts a summary of the heat storage rate for all of the cases investigated in this section. The retrieved data reveals that the heat storage rates for Cases A1, A2, A3, and A4 are 11.45, 11.48, 11.41, and 11.36 W, respectively. As a result, varying the spacing between fin sections from that in Case A4 would result in faster heat storage rates of around 0.8, 1.1, and 0.4% in Cases A1, A2, and A3, respectively. In conclusion, the spacings between the dimple-fin sections should be optimized in accordance with the thermal performance indicators (i.e., liquid-fraction evolution, temperature distribution, and heat storage rate) to effectively boost the melting enhancement potential of dimple fins.

5.5 Impact of applying the staggered distribution of fins

As yet, the effect of dimple fins with an inline fin distribution on the thermofluidic behavior of PCM during melting mode was investigated. This section is to examine the effect of employing a staggered fin distribution on the liquid fraction and temperature fields, as well as overall heat storage rates. Three distinct fin configurations of inline and staggered arrangements are studied in this regard as shown in Fig. 20. The best-case considering the optimal fin spacing based on the aromatic method (Case A2) was considered as the reference case. Inline fin arrangement is considered in Case A2 while staggered arrangement is considered in Cases A2.1 and A2.2.

Figure 21 compares the influence of the inline and staggered fin configuration on the PCM liquid-fraction evolution contours exactly 1 hour after the melting initiation. Comparing the different cases in the figure shows that employing staggered distribution on four of the fin sections in Case A2 enables larger melting layers (red zones) to form between and around the fin sections. This behavior would be attributed to the fact that adjusting fin arrangement along the circumferential direction produces better space for natural convective currents to move through, re-
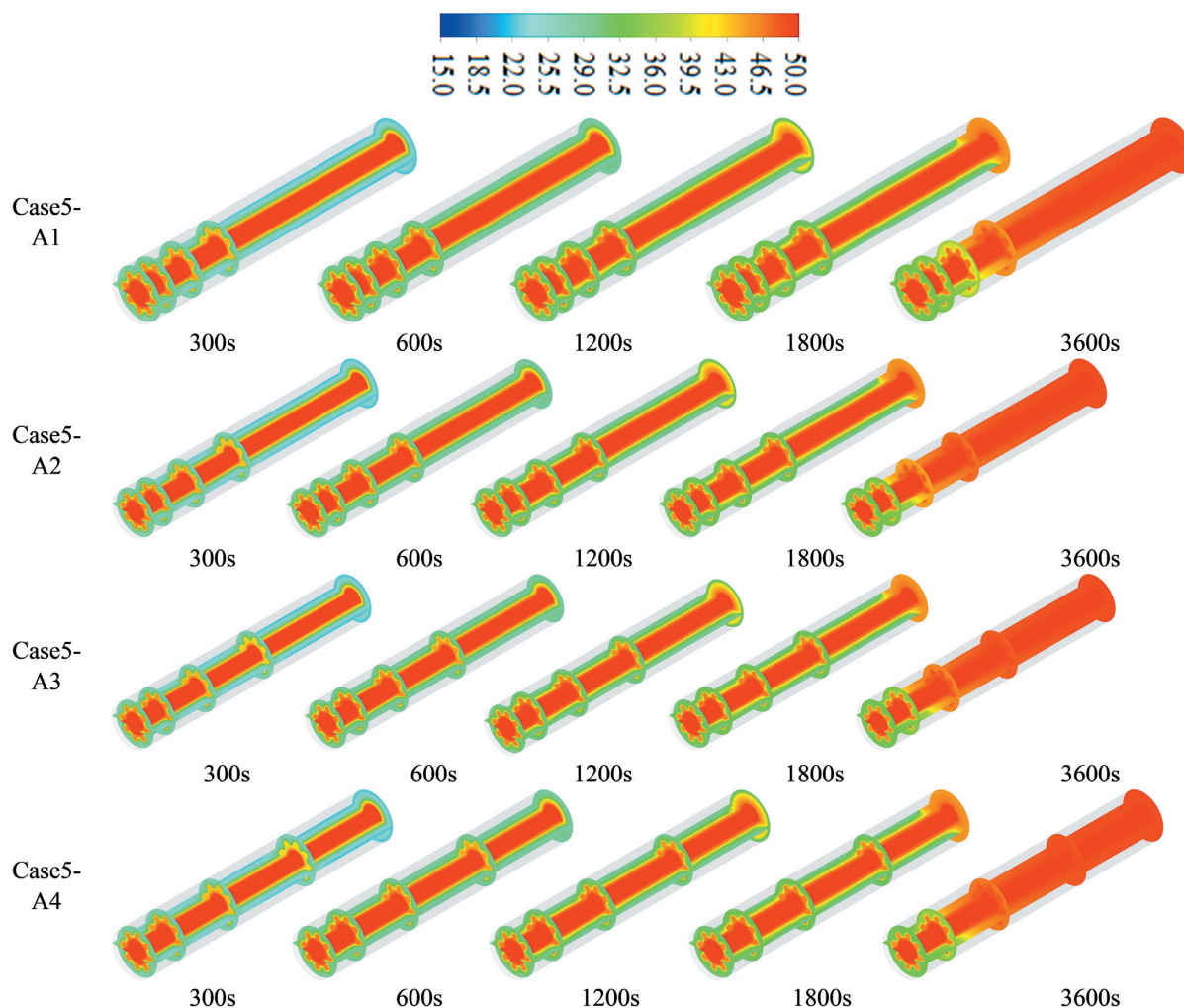
Figure 18: The timewise isotherm distribution for Case 5 with fin spacings being optimized based on the aromatic algorithm.
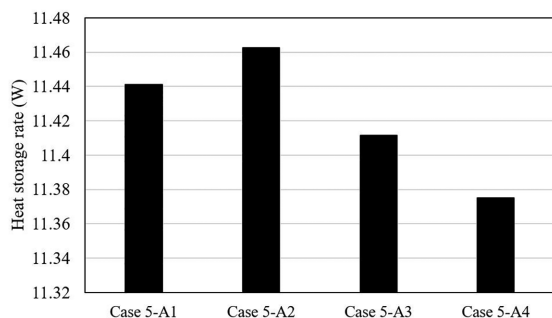

Figure 19: The overall heat storage rates for Case 5 with fin spacings being optimized based on the aromatic algorithm.

sulting in larger heat diffusions across the PCM layers involved. As shown in Fig. 21, the particular fin arrangement of Case A2.2 drives the best liquid-fraction evolution during the melting mode.

The isotherm distributions for the three Cases A2, A2.1, and A2.2 explored in this section are shown in Fig. 22 for six melting intervals ranging from 300 to 3600 s. The isotherms overall melting intervals demonstrate that using the staggered arrangement on four fin sections in Case A2.2 results in greater heat diffusion across the PCM domain compared to using the staggered arrange-

ment on only three fin sections in Case A2.1. As a result, warmer PCM layers (red zones) would emerge throughout the melting duration in the cases with staggered arrangements as compared to the inline arrangement in the reference Case A2.

Figure 23 summarizes the heat storage rate for each example examined in this section. The obtained data indicate that the heat storage rates for Cases A2, A2.1, and A2.2 are, respectively, 11.44, 11.48, and 11.49 W. That implies that applying the staggered arrangement to four and three fin sections results in heat storage rates of approximately 0.5 and 1.0% faster in Cases A2.1 and A2.2, respectively.

6. Conclusions

Dimple-shaped fins were numerically examined in this work as innovative fin configurations to look at how well the melting behavior of PCM can be improved in a shell and tube containment. The goal was to test different fin configurations while optimizing their geometric parameters such as fin dimensions, positions, and distributions to facilitate faster heat storage rates. There were five scenarios investigated to reach the optimum array of dimple fins while keeping the total volume of fins constant in all scenarios to enable meaningful performance comparisons. These scenarios were: (i) determining the optimal number of dimple fins to utilize; (ii) finding the best position for the first fin section; (iii) seeking
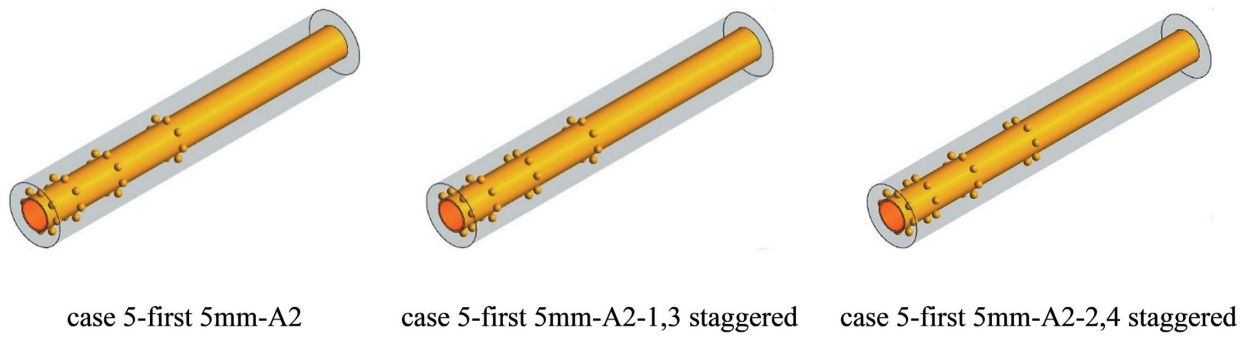
case 5-first 5mm-A2   case 5-first 5mm-A2-1,3 staggered   case 5-first 5mm-A2-2,4 staggered

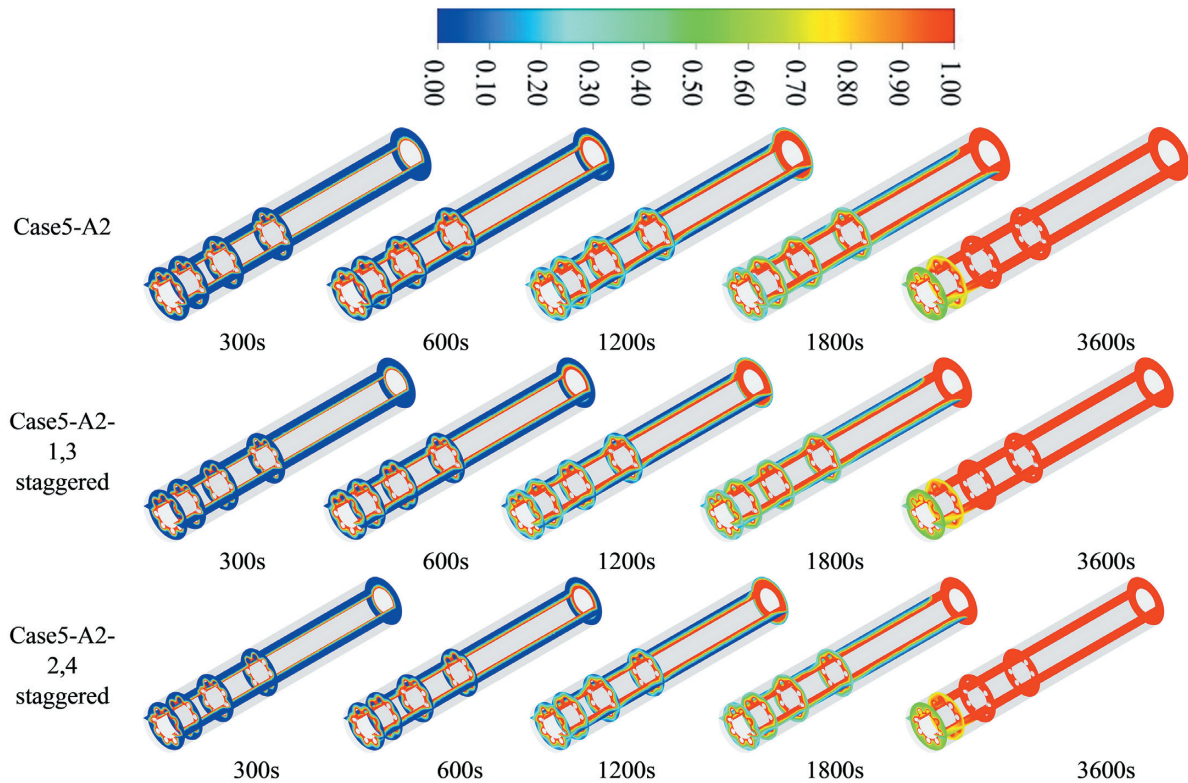**Figure 20:** Schematic of dimple fins of Case 5 with inline and staggered fin arrangements.

Figure 21: The timewise liquid-fraction evolution for Case 5 with inline and staggered arrangements of dimple fins.

the optimal fin spacing; (iv) determining the optimal fin spacing using the aromatic algorithm; and (v) employing staggered fin arrangement to optimize the enhancement potential. The key findings can be summarized as follows:

(i) Employing a larger number of dimple fins, particularly at high numbers such as 24 and 32 fins, offers an increase in the size of melting layers and faster heat storage rates. The results imply that increasing the number of dimple fins from 0 to 8, 16, 20, and 24 fins would result in heat storage rates of about 7.1, 8.4, and 8.7% faster than they would be otherwise.

(ii) Making the spacing of the first fin section smaller for values like 5 and 10 mm can make dimple fin arrays more effective at boosting heat transfer rates through natural convection. This makes them more useful for this purpose. reveal that reducing the spacing for the first fin section from 50 mm to 40, 30, 20, 10, and 5 mm would result in faster heat storage rates by about 0.5, 1.0, 1.4, and 2.0%.

(iii) Other than the first fin section, the spacing between fin sections should be optimized for better melting enhancement rates. The results show that increasing the spacing between fin sections to 20, 30, 40, and 50 mm results in heat storage rates that are 0.7, 0.9, 1.2, and 0.5% faster than if the spacing was kept constant at 10 mm.

(iv) Optimizing the fin spacings to different values based on the aromatic algorithm can further support the enhancement potential of dimple fins by improving the efficiency of local natural convection. For example, applying spacings such as 5, 25, 60, and 110 mm for the first, second, third, and fourth fin sections can improve the heat storage rate by 1.1% more than it would be if the spacing between the fin sections is kept constant at 10 mm.

(v) Employing the staggered fin distribution with the optimal fin spacing based on the aromatic method can further improve the melting enhancement. Compared to the inline arrangement, the results indicate that applying the stag-
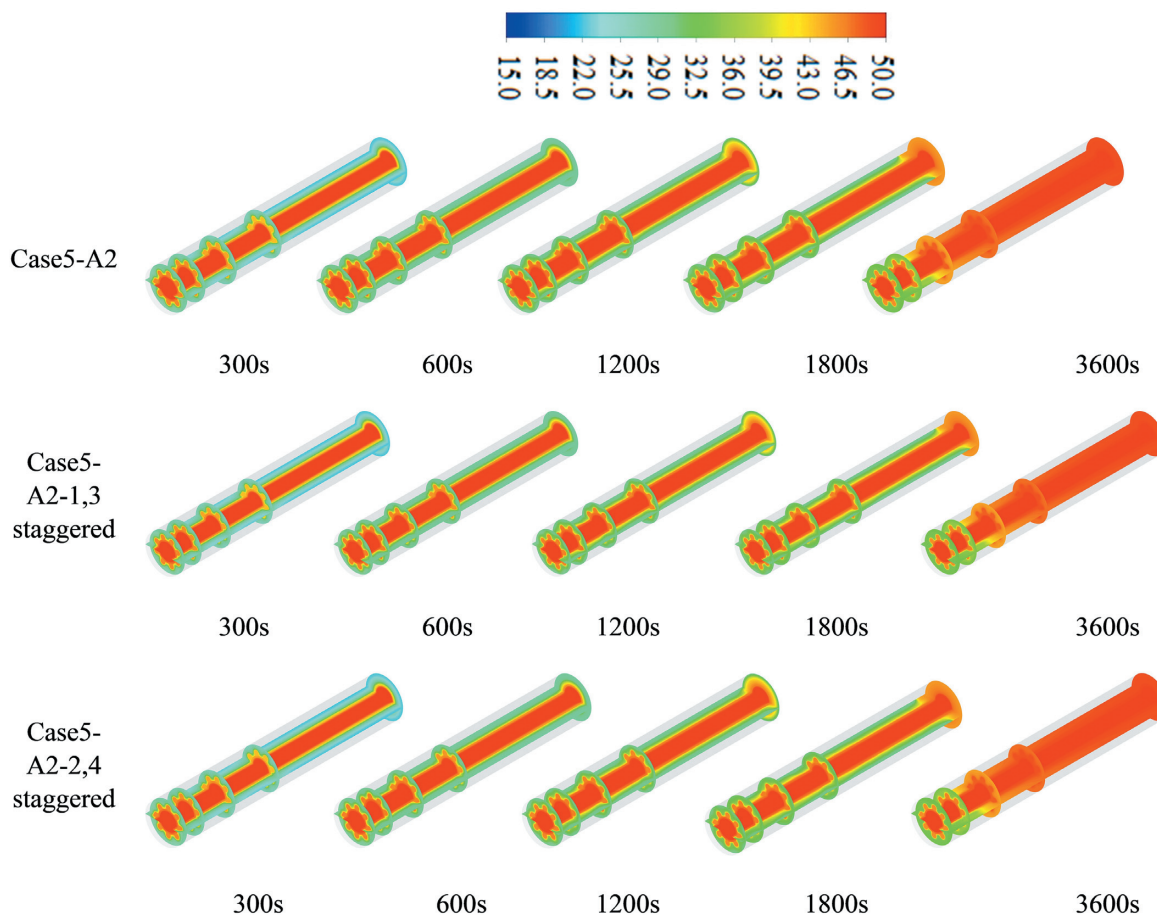
Figure 22: The timewise isotherm distribution for Case 5 with inline and staggered arrangements of dimple fins.
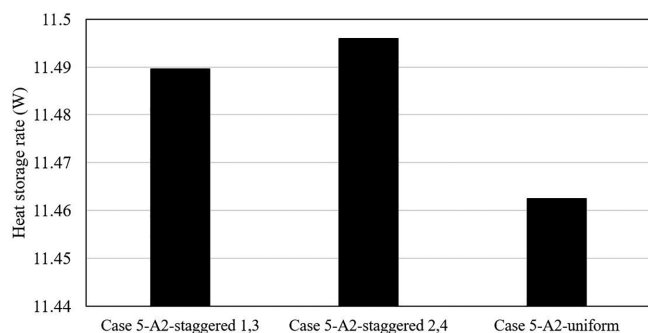

Figure 23: The overall heat storage rates for Case 5 with inline and staggered arrangements of dimple fins.

gered arrangement to three fin sections results in higher heat storage rates by about 1.0%. The heat storage rate improves by almost 12% for the best case compared with that of the no-fin case.

Acknowledgments

Conflict of interest statement

None declared.

References

Abdulateef, A. M., Mat, S., Abdulateef, J., Sopian, K., & Al-Abidi, A. A. (2018a). Geometric and design parameters of fins employed for enhancing thermal energy storage systems: A review. *Renewable and Sustainable Energy Reviews*, **82**, 1620–1635. https://doi.org/10.1016/j.rser.2017.07.009.

Abdulateef, A. M., Abdulateef, J., Mat, S., Sopian, K., Elhub, B., & Mussa, M. A. (2018b). Experimental and numerical study of solidifying phase-change material in a triplex-tube heat exchanger with longitudinal/triangular fins. *International Communications in Heat and Mass Transfer*, **90**, 73–84. https://doi.org/10.1016/j.icheatmasstransfer.2017.10.003.

Ali, H. M. (2019). Applications of combined/hybrid use of heat pipe and phase change materials in energy storage and cooling systems: A recent review. *Journal of Energy Storage*, **26**, 100986. https://doi.org/10.1016/j.est.2019.100986.

Brent, A. D., Voller, V. R., & Reid, K. J. (1988). Enthalpy-porosity technique for modeling convection-diffusion phase change: Application to the melting of a pure metal. *Numerical Heat Transfer, Part A Applications*, **13**, 297–318. https://doi.org/10.1080/10407788808913615.

Cabeza, L. F. (2021). *Advances in thermal energy storage systems: Methods and applications*, Elsevier.

Dincer, I., & Rosen, M. A. (2021). *Thermal energy storage systems and applications*, John Wiley & Sons.

Dong, Yu., Liu, Y., Wang, D., Wang, Y., Du, Hu., & Liu, J. (2020). Review of latent thermal energy storage systems for solar air-conditioning systems. *International Journal of Energy Research*, **44**, 669. https://doi.org/10.1002/er.4960.

Fadl, M., & Eames, P. C. (2019). Numerical investigation of the influence of mushy zone parameter amush on heat transfer characteristics in vertically and horizontally oriented thermal energy storage systems. *Applied Thermal Engineering*, **151**, 90–99. https://doi.org/10.1016/j.applthermaleng.2019.01.102.

Ghalambaz, M., Mahdi, J. M., Shafaghat, A., Eisapour, A. H., Younis, O., Talebizadeh Sardari, P., & Yaici, W. (2021a). Effect of twisted fin array in a triple-tube latent heat storage system during the charging mode. *Sustainability*, **13**, 2685. https://doi.org/10.3390/su13052685.

Ghalambaz, M., Mohammed, H. I., Mahdi, J. M., Eisapour, A. H., Younis, O., Ghosh, A., Talebizadehsardari, P., & Yaici, W. (2021b). Intensifying the charging response of a phase-change material with twisted fin arrays in a shell-and-tube storage system. *Energies*, **14**, 1619. https://doi.org/10.3390/en14061619.

Gong, D., Wei, C., Xie, D., & Tang, Y. (2022). Ultrasmall antimony nanodots embedded in carbon nanowires with three-dimensional porous structure for high-performance potassium dual-ion batteries. *Chemical Engineering Journal*, **431**, 133444. https://doi.org/10.1016/j.cej.2021.133444.

Guo, J., Wang, X., Yang, Bo., Yang, X., & Li, M. J. (2022). Thermal assessment on solid-liquid energy storage tube packed with non-uniform angled fins. *Solar Energy Materials and Solar Cells*, **236**, 111526. https://doi.org/10.1016/j.solmat.2021.111526.

Huang, Y., Cao, D., Sun, D., & Liu, X. (2022). Experimental and numerical studies on the heat transfer improvement of a latent heat storage unit using gradient tree-shaped fins. *International Journal of Heat and Mass Transfer*, **182**, 121920. https://doi.org/10.1016/j.ijheatmasstransfer.2021.121920.

Huang, Y., & Liu, X. (2021). Charging and discharging enhancement of a vertical latent heat storage unit by fractal tree-shaped fins. *Renewable Energy*, **174**, 199–217. https://doi.org/10.1016/j.renene.2021.04.066.

Lacroix, M. (1993). Study of the heat transfer behavior of a latent heat thermal energy storage unit with a finned tube. *International Journal of Heat and Mass Transfer*, **36**, 2083–2092. https://doi.org/10.1016/S0017-9310(05)80139-5.

Lamrani, B., Johannes, K., & Kuznik, F. (2021). Phase change materials integrated into building walls: An updated review. *Renewable and Sustainable Energy Reviews*, **140**, 110751. https://doi.org/10.1016/j.rser.2021.110751.

Lane, G. A. (1983). Solar heat storage: Latent heat materials. CRC Press.

Li, Z. X., Al-Rashed, A. A. A. A., Rostamzadeh, M., Kalbasi, R., Shahsavar, A., & Afrand, M. (2019). Heat transfer reduction in buildings by embedding phase change material in multi-layer walls: Effects of repositioning, thermophysical properties and thickness of PCM. *Energy Conversion and Management*, **195**, 43–56. https://doi.org/10.1016/j.enconman.2019.04.075.

Mahdi, J. M., Mohammed, H. I., Hashim, E. T., Talebizadehsardari, P., & Nsofor, E. C. (2020). Solidification enhancement with multiple PCMs, cascaded metal foam and nanoparticles in the shell-and-tube energy storage system. *Applied Energy*, **257**, 113993. https://doi.org/10.1016/j.apenergy.2019.113993.

Mahdi, J. M., Mohammed, H. I., Talebizadehsardari, P., Ghalambaz, M., Sh. Majdi, H., Khan, A., Yaici, W., & Giddings, D. (2021a). Simultaneous and consecutive charging and discharging of a PCM-based domestic air heater with metal foam. *Applied Thermal Engineering*, **197**, 117408. https://doi.org/10.1016/j.applthermaleng.2021.117408.

Mahdi, J. M., Pal Singh, R., Taqi Al-Najjar, H. M., Singh, S., & Nsofor, E. C. (2021b). Efficient thermal management of the photovoltaic/phase change material system with innovative exterior metal-foam layer. *Solar Energy*, **216**, 411–427. https://doi.org/10.1016/j.solener.2021.01.008.

Mahdi, J. M., Mohammed, H. I., & Talebizadehsardari, P. (2021c). A new approach for employing multiple PCMs in the passive thermal management of photovoltaic modules. *Solar Energy*, **222**, 160–174. https://doi.org/10.1016/j.solener.2021.04.044.

Mahdi, J. M., & Nsofor, E. C. (2017). Melting enhancement in triplex-tube latent thermal energy storage system using nanoparticles-fins combination. *International Journal of Heat and Mass Transfer*, **109**, 417–427. https://doi.org/10.1016/j.ijheatmasstransfer.2017.02.016.

Mahdi, J. M., & Nsofor, E. C. (2018a). Accelerated melting of PCM in energy storage systems via novel configuration of fins in the triplex-tube heat exchanger. *International Journal of Heat and Mass Transfer*, **124**, 663–676. https://doi.org/10.1016/j.ijheatmasstransfer.2017.02.016.

Mahdi, J. M., & Nsofor, E. C. (2018b). Solidification enhancement of PCM in a triplex-tube thermal energy storage system with nanoparticles and fins. *Applied Energy*, **211**, 975–986. https://doi.org/10.1016/j.apenergy.2017.11.082.

Mahmoud, M., Mohammed, H., Mahdi, J., Bokov, D., Ben Khedher, N., Alshammari, N., Talebizadehsardari, P., & Yaici, W., (2021). Melting enhancement in a triple-tube latent heat storage system with sloped fins, *Nanomaterials*, **11**, 3153. https://doi.org/10.3390/nano11113153.

Mat, S., Al-Abidi, A. A., Sopian, K., Sulaiman, M. Y., & Mohammad, A. T. (2013). Enhance heat transfer for PCM melting in triplex tube with internal–external fins. *Energy Conversion and Management*, **74**, 223–236. https://doi.org/10.1016/j.enconman.2013.05.003.

Pan, C., Charles, J., Vermaak, N., Romero, C., Neti, S., Zheng, Y., Chen, C. H., & Bonner, R. (2018). Experimental, numerical and analytic study of unconstrained melting in a vertical cylinder with a focus on mushy region effects. *International Journal of Heat and Mass Transfer*, **124**, 1015–1024. https://doi.org/10.1016/j.ijheatmasstransfer.2018.04.009.

Pelay, U., Luo, L., Fan, Y., Stitou, D., & Rood, M. (2017). Thermal energy storage systems for concentrated solar power plants. *Renewable and Sustainable Energy Reviews*, **79**, 82–100. https://doi.org/10.1016/j.rser.2017.03.139.

Rea, J. E., Oshman, C. J., Olsen, M. L., Hardin, C. L., Glatzmaier, G. C., Siegel, N. P., Parilla, P. A., Ginley, D. S., & Toberer, E. S. (2018). Performance modeling and techno-economic analysis of a modular concentrated solar power tower with latent heat storage. *Applied Energy*, **217**, 143–152. https://doi.org/10.1016/j.apenergy.2018.02.067.

Ritchie, H., Roser, M., & Rosado, P. (2020). CO_2 and greenhouse gas emissions. *Our World in Data*. https://ourworldindata.org/co2-and-other-greenhouse-gas-emissions.

Rubitherm GmbH. (n.d.). RT35 data sheet. https://www.rubitherm.eu.

Sadeghianjahromi, A., & Wang, C. C. (2021). Heat transfer enhancement in fin-and-tube heat exchangers—A review on different mechanisms. *Renewable and Sustainable Energy Reviews*, **137**, 110470. https://doi.org/10.1016/j.rser.2020.110470.

Saffari, M., De Gracia, A., Fernández, C., Belusko, M., Boer, D., & Cabeza, LF. (2018). Optimized demand side management (DSM) of peak electricity demand by coupling low temperature thermal

energy storage (TES) and solar pV. *Applied Energy*, **211**, 604–616. https://doi.org/10.1016/j.apenergy.2017.11.063.

Sardari, P. T., Grant, D., Giddings, D., Walker, GS., & Gillott, M. (2019). Composite metal foam/PCM energy store design for dwelling space air heating. *Energy Conversion and Management*, **201**, 112151. https://doi.org/10.1016/j.enconman.2019.112151.

Sciacovelli, A., Gagliardi, F., & Verda, V. (2015). Maximization of performance of a PCM latent heat storage system with innovative fins. *Applied Energy*, **137**, 707–715. https://doi.org/10.1016/j.apenergy.2014.07.015.

Shahsavar, A., Goodarzi, A., Mohammed, H. I., Shirneshan, A., & Talebizadehsardari, P. (2020). Thermal performance evaluation of non-uniform fin array in a finned double-pipe latent heat storage system. *Energy*, **193**, 116800. https://doi.org/10.1016/j.energy.2019.116800.

Singh, R. P., Xu, H., Kaushik, S. C., Rakshit, D., & Romagnoli, A. (2019). Effective utilization of natural convection via novel fin design & influence of enhanced viscosity due to carbon nano-particles in a solar cooling thermal storage system. *Solar Energy*, **183**, 105–119. https://doi.org/10.1016/j.solener.2019.03.005.

Sun, X., Mohammed, H. I., Tiji, M. E., Mahdi, J. M., Sh. Majdi, H., Wang, Z., Talebizadehsardari, P., & Yaici, W. (2021). Investigation of heat transfer enhancement in a triple TUBE latent heat storage system using circular fins with inline and staggered arrangements. *Nanomaterials*, **11**, 2647. https://doi.org/10.3390/nano11102647.

Talebizadehsardari, P., Mohammed, H. I., Mahdi, J. M., Gillott, M., Walker, G. S., Grant, D., & Giddings, D. (2021a). Effect of airflow channel arrangement on the discharge of a composite metal foam-phase change material heat exchanger. *International Journal of Energy Research*, **45**, 2593–2609. https://doi.org/10.1002/er.5949.

Talebizadehsardari, P., Mahdi, J. M., Mohammed, H. I., Moghimi, M. A., Hossein Eisapour, A., & Ghalambaz, M. (2021b). Consecutive charging and discharging of a PCM-based plate heat exchanger with zigzag configuration. *Applied Thermal Engineering*, **193**, 116970. https://doi.org/10.1016/j.applthermaleng.2021.116970.

Tang, S. Z., Tian, H. Q., Zhou, J. J., & Li, H. (2021). Evaluation and optimization of melting performance in a horizontal thermal energy storage unit with non-uniform fins. *Journal of Energy Storage*, **33**, 102124. https://doi.org/10.1016/j.est.2020.102124.

Velraj, R., Seeniraj, R. V., Hafner, B., Faber, C., & Schwarzer, K. Experimental analysis and numerical modelling of inward solidification on a finned vertical tube for a latent heat storage unit. *Solar Energy*, (1997). **60**, 281–290. https://doi.org/10.1016/S0038-092X(96)00167-3.

Wang, Y., Li, C., Zhang, Y., Yang, M., Li, B., Dong, L., & Wang, J. (2018). Processing characteristics of vegetable oil-based nanofluid MQL for grinding different workpiece materials. *International Journal of Precision Engineering and Manufacturing-Green Technology*, **5**, 327–339. https://doi.org/10.1007/s40684-018-0035-4.

Wu, Y., Zhao, Y., Han, X., Jiang, G., Shi, J., Liu, P., Khan, M. Z., Huhtinen, H., Zhu, J., Jin, Z., & Yamada, Y. (2021a). Ultra-fast growth of cuprate superconducting films: Dual-phase liquid assisted epitaxy and strong flux pinning. *Materials Today Physics*, **18**, 100400. https://doi.org/10.1016/j.mtphys.2021.100400.

Wu, X., Li, C., Zhou, Z., Nie, X., Chen, Y., Zhang, Y., Cao, H., Liu, Bo., Zhang, N., Said, Z., Debnath, S., Jamil, M., Ali, H. M., & Sharma, S. (2021b). Circulating purification of cutting fluid: An overview. *The International Journal of Advanced Manufacturing Technology*, **117**, 2565–2600. https://doi.org/10.1007/s00170-021-07854-1.

Xu, Y., Chen, X., Zhang, H., Yang, F., Tong, L., Yang, Y., Yan, D., Yang, A., Yu, M., Liu, Z., & Wang, Y. (2022). Online identification of battery model parameters and joint state of charge and state of health estimation using dual particle filter algorithms. *International Journal of Energy Research*, 1–38. https://doi.org/10.1002/er.8541.

Yang, X., Guo, J., Yang, Bo., Cheng, H., Wei, P., & He, Y. L. (2020). Design of non-uniformly distributed annular fins for a shell-and-tube thermal energy storage unit. *Applied Energy*, **279**, 115772. https://doi.org/10.1016/j.apenergy.2020.115772.

Yang, Yi., Zhu, H., Xu, X., Bao, L., Wang, Y., Lin, H., & Zheng, C. (2021). Construction of a novel lanthanum carbonate-grafted ZSM-5 zeolite for effective highly selective phosphate removal from wastewater. *Microporous and Mesoporous Materials*, **324**, 111289. https://doi.org/10.1016/j.micromeso.2021.111289.

Yang, X., Wang, X., Liu, Z., Luo, X., & Yan, J. (2022a). Effect of fin number on the melting phase change in a horizontal finned shell-and-tube thermal energy storage unit. *Solar Energy Materials and Solar Cells*, **236**, 111527. https://doi.org/10.1016/j.solmat.2021.111527.

Yang, Yi., Wang, Y., Zheng, C., Lin, H., Xu, R., Zhu, H., Bao, L., & Xu, X. (2022b). Lanthanum carbonate grafted ZSM-5 for superior phosphate uptake: investigation of the growth and adsorption mechanism. *Chemical Engineering Journal*, **430**, 133166. https://doi.org/10.1016/j.cej.2021.133166.

Yu, C., Zhang, X., Chen, Xi., Zhang, C., & Chen, Y. (2020). Melting performance enhancement of a latent heat storage unit using gradient fins. *International Journal of Heat and Mass Transfer*, **150**, 119330. https://doi.org/10.1016/j.ijheatmasstransfer.2020.119330.

Zhang, D., Li, C., Zhang, Y., Jia, D., & Zhang, X. (2015). Experimental research on the energy ratio coefficient and specific grinding energy in nanoparticle jet MQL grinding. *The International Journal of Advanced Manufacturing Technology*, **78**, 1275–1288. https://doi.org/10.1007/s00170-014-6722-6.

Zhang, X., Tang, Y., Zhang, F., & Lee, C. S. (2016). A novel aluminum–graphite dual-ion battery. *Advanced Energy Materials*, **6**, 1502588. https://doi.org/10.1002/aenm.201502588.

Zhang, J., Li, C., Zhang, Y., Yang, M., Jia, D., Liu, G., Hou, Y., Li, R., Zhang, N., Wu, Q., & Cao, H. (2018). Experimental assessment of an environmentally friendly grinding process using nanofluid minimum quantity lubrication with cryogenic air. *Journal of Cleaner Production*, **193**, 236–248. https://doi.org/10.1016/j.jclepro.2018.05.009.

Zhang, C., Li, J., & Chen, Y. (2020). Improving the energy discharging performance of a latent heat storage (LHS) unit using fractal-tree-shaped fins. *Applied Energy*, **259**, 114102. https://doi.org/10.1016/j.apenergy.2019.114102.